

Supplementary Materials

Phthalonitrile melting point prediction enabled by multi-fidelity learning

**Beijian Xu^{1,#}, Xiao Hu^{1,#}, Haoxiang Lan^{1,#}, Tianyi Wang¹, Xin-Yao Xu¹, Chongyin Zhang^{2,*},
Jiaping Lin^{1,*}, Liquan Wang^{1,*}, Lei Du¹**

¹Shanghai Key Laboratory of Advanced Polymeric Materials, Key Laboratory of Specially Functional Polymeric Materials and Related Technology (Ministry of Education), School of Materials Science and Engineering, East China University of Science and Technology, Shanghai 200237, China.

²Shanghai Aerospace Equipment Manufacturing Co., Ltd., Shanghai 200245, China.

#Authors contributed equally.

***Correspondence to:** Dr. Chongyin Zhang, Shanghai Aerospace Equipment Manufacturing Co., Ltd., Huaning Road 100, Minhang District, Shanghai 200245, China. E-mail: chongyin1022@163.com; Prof. Jiaping Lin, Prof. Liquan Wang, Shanghai Key Laboratory of Advanced Polymeric Materials, Key Laboratory of Specially Functional Polymeric Materials and Related Technology (Ministry of Education), School of Materials Science and Engineering, East China University of Science and Technology, Meilong Road 130, Xuhui District, Shanghai 200237, China. E-mail: jlin@ecust.edu.cn; lq_wang@ecust.edu.cn

Contents

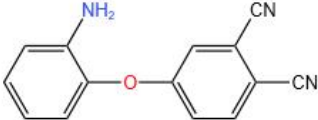
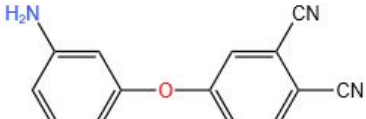
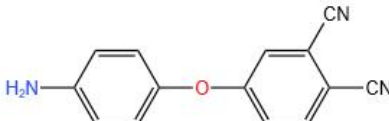
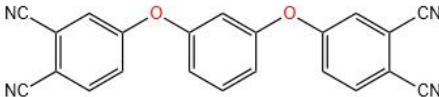
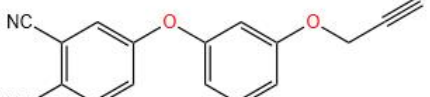
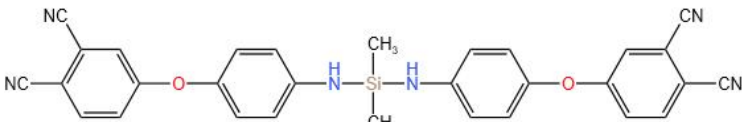
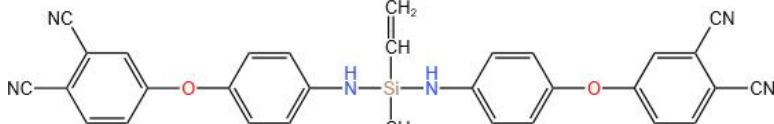
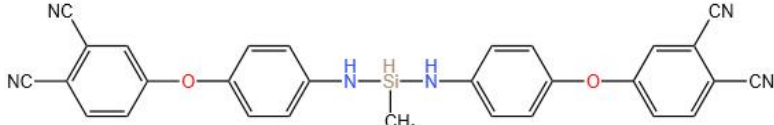
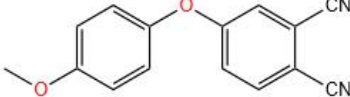
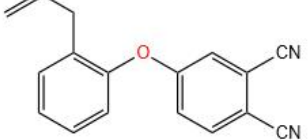
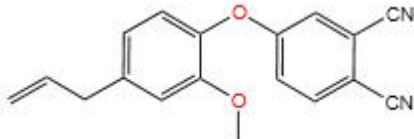
1. Collection of Experimentally Measured Melting Points of Phthalonitriles	S3
2. Generation of Candidate Space for Phthalonitriles through Gene Combination	S11
3. <i>t</i> -SNE Process and Random Sampling	S14
4. Molecular Dynamic Simulation of Phthalonitrile Melting Points	S22
5. Gaussian Process Regression	S25
6. Constructing Models by Gaussian Process Regression	S27
7. Graph Machine Learning, MPNN and MEGNet	S30
References	S355

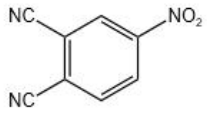
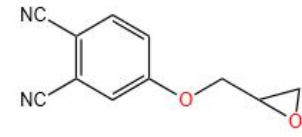
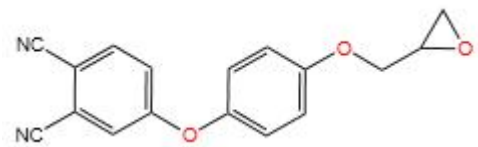
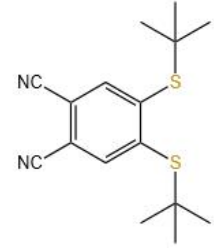
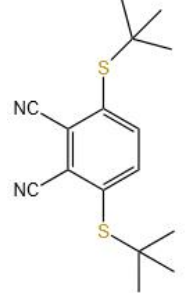
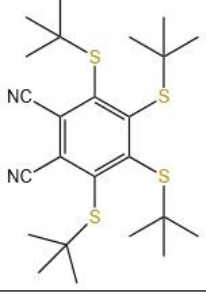
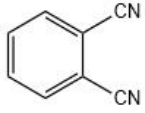
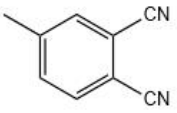
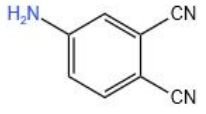
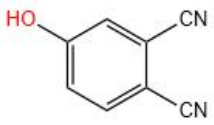
1. Collection of Experimentally Measured Melting Points of Phthalonitriles

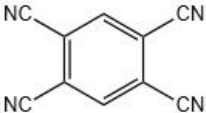
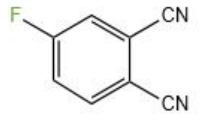
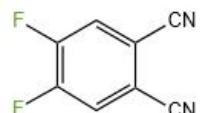
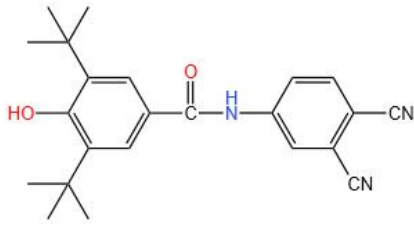
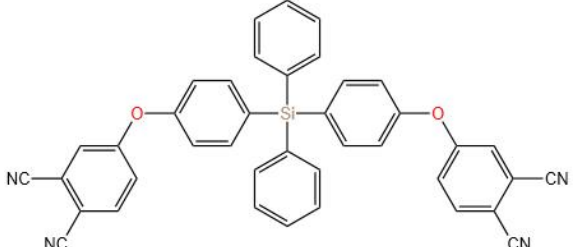
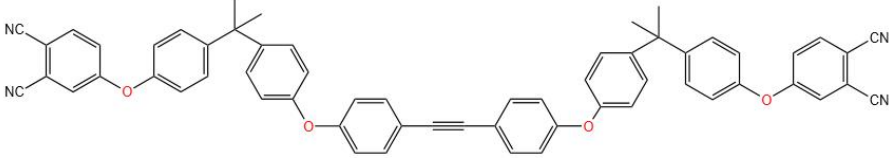
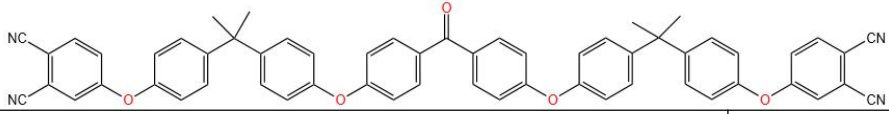
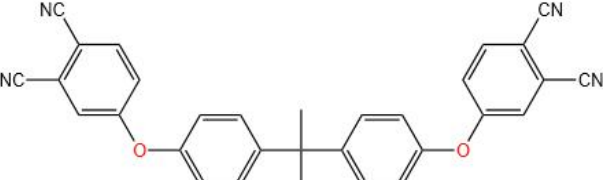
Experimentally measured melting points are regarded as high-fidelity data for machine learning. We, therefore, collected melting point data of phthalonitriles extensively from the literature. We found that phthalonitrile compounds have been recorded with varying melting points due to several factors: 1) different experimenters measured melting points under distinct particular environments or physical conditions for their specific experimental purposes; 2) in some studies, due to limitations in instrument precision, melting points were only reported as ranges (e.g., 180-200 °C) or as approximate values (e.g., ≈ 200 °C); 3) the phthalonitrile mixtures with varied components exhibited the same melting point.

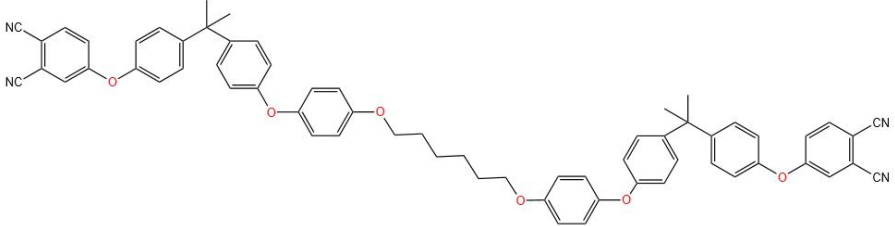
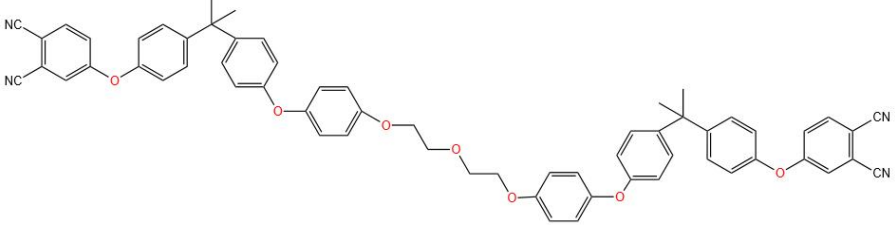
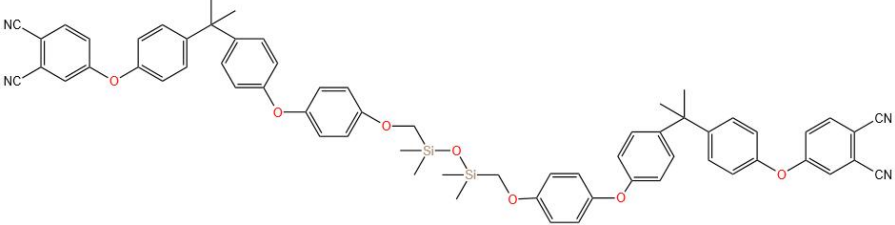
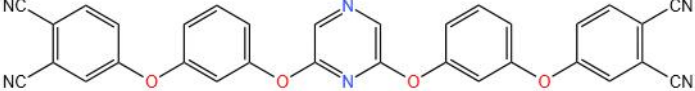
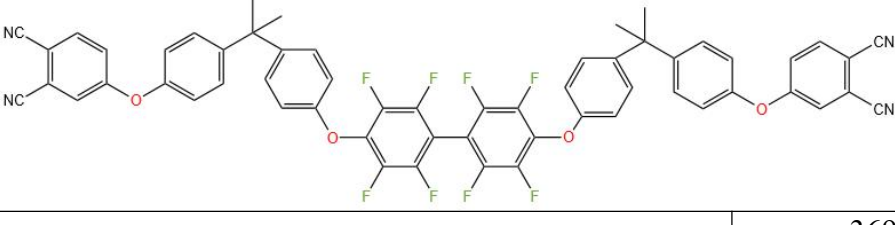
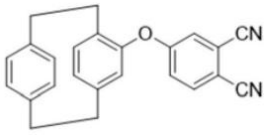
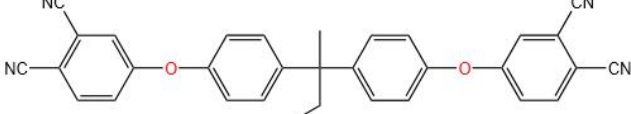
Collecting rules are as follows: (1) Substances collected must belong to the phthalonitrile category, which possesses a clearly defined or queryable structure. (2) Substances collected must have experimentally determined melting point values documented in the literature or other referenced sources. Note that the melting point here must be a pure substance under standard experimental conditions. The data determined under particular conditions, expressed as ranges, or measured for mixtures are unacceptable. (3) Since this study focuses on small molecules, molecules with more than 200 atoms will not be considered. Ultimately, we found 58 phthalonitrile structures complied with the prescribed rules and collected their corresponding melting points. The phthalonitrile structures and melting points are collected from ref. [1-25] and presented in Table S1.

Supplementary Table 1 Phthalonitrile structures and melting points collected from the literature^[1-25]

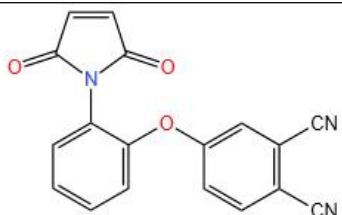
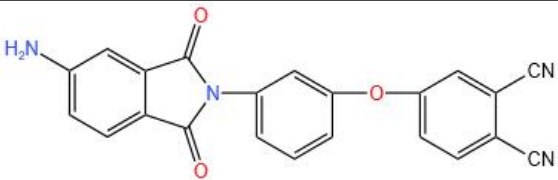
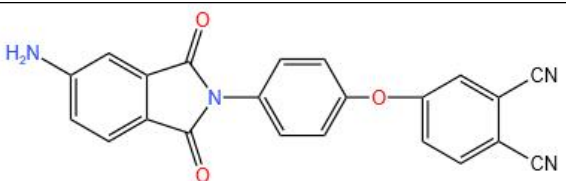
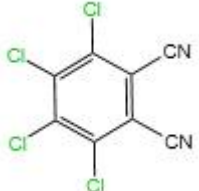
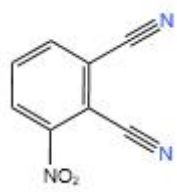
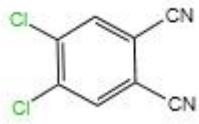
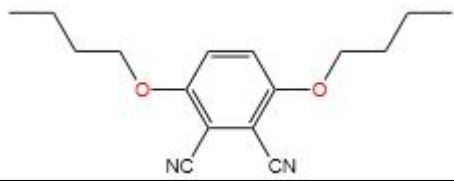
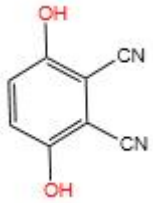
No.	Structure	Melting Point (K)
1		395.26
2		446.99
3		408.83
4		458
5		390
6		332
7		313
8		315
9		355.9
10		334
11		371

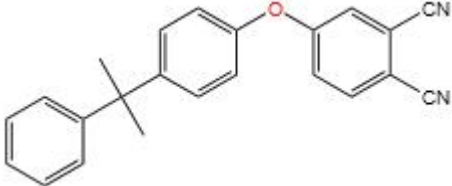
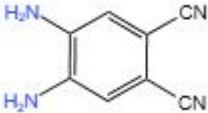
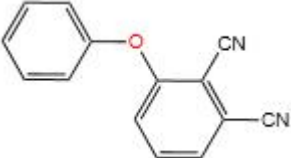
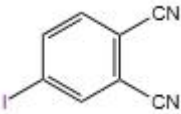
12		409.5
13		386
14		368
15		437
16		450.5
17		490
18		414
19		393
20		454
21		491

22		541
23		373
24		387
25		490.5
26		495.5
27		464
28		348
29		348
30		468

31		323
32		333
33		308
34		436
35		369
36		406
37		504
38		440

39		430
40		432
41		468
42		333
43		359
44		294
45		483.4
46		380.4

47		473.8
48		483
49		513
50		525
51		435
52		453
53		463
54		540

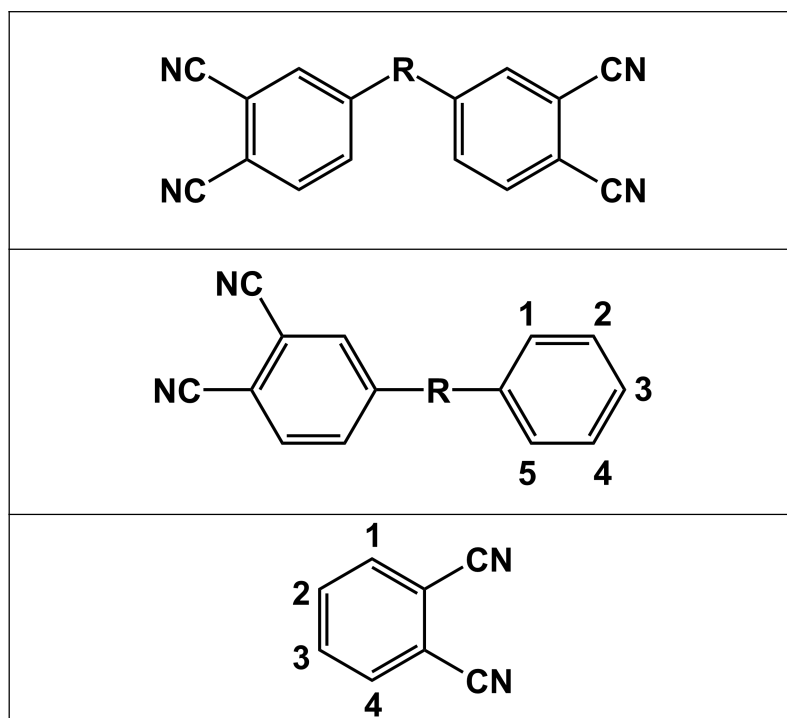
55		364
56		549
57		390
58		413

2. Generation of Candidate Space for Phthalonitriles through Gene Combination

The experimentally measured melting points in Table S1 cannot support machine learning (ML) well due to the small volume of data. However, continuously searching phthalonitrile structures and corresponding melting points from reported experimental works is tedious and inefficient. There has been progress in automatic data mining by computer in recent years; for instance, Wang et al.^[26] developed an automated literature mining workflow that extracted 2531 pieces of data of interest from 14425 articles within 3 hours. However, this technology still has limitations and does not apply to this work.

Therefore, we aspire to artificially create specific relevant structures for further research by leveraging the concepts associated with material gene combinations. Gene combination simplifies the synthesis of substances into a random combination of chemical units (including spacer and substituent groups) within a structural template. In this study, we defined three structural templates for phthalonitrile (see Table S2), identified the positions of substitutable points in the structures, and selected several chemical units covering H, C, N, O, F, Si, P, S, and Cl elements for the combination. Chemical units involved in this work are listed in Table S3. Note that attachment sites of chemical units are indicated by "*" (see Table S3), and the numbers on the structural template represent the designated positions where substituents can be replaced (see Table S2).

Supplementary Table 2 Molecular templates considered in this work



Supplementary Table 3 Chemical units involved in gene combination

Spacer (R Group)	Substituent
O	*O
S	*C
C()=O	*C=C
OC(=O)O	*C(=O)OC
O[Si](C)(C)O	*F
Oc1ccc(O)cc1	*Cl
OP(=O)(O)O	*OC
NC()=O	*N
S() (=O) =O	*[N+](=O)[O-]
C(C(F)(F)F)C(F)(F)F	*c1ccccc1
\	*C(=O)O

RDKit tool was used to implement gene combinations. Such an implement can generate an enormous chemical structure candidate space. Suppose the number of considered chemical units increases to 100. In that case, the number of substituents allowed on the benzene ring is 5, and various isomers are considered; the potential chemical structure obtained through gene combination will exceed 200 million. Such a candidate space is a huge burden to process. To avoid this, we imposed restrictions on the number of chemical units and substitution positions. Furthermore, to guarantee that the obtained structures are relatively rational and stable, we initially screened the candidate space to eliminate unreasonable structures. Finally, we obtained a candidate space containing 148964 phthalonitrile structures for further investigation.

3. *t*-SNE Process and Random Sampling

t-distributed Stochastic Neighbor Embedding (*t*-SNE) is a machine learning algorithm proposed by Geoffrey Hinton and Laurens van der Maaten in 2008, designed for dimensionality reduction and visualization of high-dimensional data. By preserving the similarity relationships between data points in a high-dimensional space and mapping them to a low-dimensional space, this approach facilitates a more intuitive observation and understanding of the structure, clustering, and similarity of the data.

In section S2, we obtained a vast candidate space of phthalonitrile structures, but studying all these at once is impractical. Therefore, selecting a subset as representative is a natural choice. In this study, we aim for our proposed machine learning model to predict the melting points of a wide range of phthalonitrile substances, requiring the dataset to include diverse structures with broad coverage in the candidate space. Since manual selection is unrealistic, the *t*-SNE method comes to our mind. We utilized the Mordred tool to calculate descriptors for all structures in the candidate space and removed illegal strings from the descriptors. Then, we directly applied *t*-SNE for dimensionality reduction and visualized the results in a two-dimensional space. In this space, each structure is represented as a coordinate point. If the two points are close, we can say that these two phthalonitriles have similar structures.

Our sampling aims to achieve the opposite, which means that we are attempting to distribute all selected points evenly throughout the entire space to meet the requirement of obtaining a more diverse dataset. Various methods can be employed for sampling; here, we adopted a geometric method, dividing the entire region into several blocks and randomly sampling from each block until the required number of samples was reached. Ultimately, we extracted 200 sample points, and their

distribution proved even and extensive. The sampled structures are listed in Table S4.

Supplementary Table 4 Phthalonitrile structures selected from the candidate space.

No.	SMILES
1	<chem>C=Cc1c(O)ccc(C(=O)c2ccc(C#N)c(C#N)c2)c1-c1ccccc1</chem>
2	<chem>Cc1cccc(Cl)c1O[Si](C)(C)Oc1cccc(C#N)c1C#N</chem>
3	<chem>COc1cc(C#N)c(C#N)c(Cc2ccccc2)c1C(=O)O</chem>
4	<chem>C=CCc1c(C#N)c(C#N)cc(CC)c1S(=O)(=O)O</chem>
5	<chem>COc1cc(OC(=O)Oc2ccc(C#N)c(C#N)c2)c(C)c(-c2ccccc2)c1</chem>
6	<chem>C=Cc1c(Cl)cc(C(=O)c2ccc(C#N)c(C#N)c2)cc1-c1ccccc1</chem>
7	<chem>COC(=O)c1cc(O[Si](C)(C)Oc2ccc(C#N)c(C#N)c2)cc(C)c1C(=O)OC</chem>
8	<chem>COC(=O)c1c(-c2ccccc2)ccc(Cl)c1Sc1cccc(C#N)c1C#N</chem>
9	<chem>N#Cc1ccc(C(=O)c2cc(-c3ccccc3)cc(-c3ccccc3)c2)cc1C#N</chem>
10	<chem>C[Si](C)(Oc1cccc(C#N)c1C#N)Oc1c(N)cc(-c2ccccc2)cc1N</chem>
11	<chem>N#Cc1cccc(OC(=O)Oc2cc(F)cc([N+](=O)[O-])c2C(=O)O)c1C#N</chem>
12	<chem>C=Cc1cc(Oc2ccc(C#N)c(C#N)c2)c(F)cc1C(=O)OC</chem>
13	<chem>COC(=O)c1cc(O[Si](C)(C)Oc2ccc(C#N)c(C#N)c2)c(C(=O)O)cc1C(=O)O</chem>
14	<chem>Cc1ccc(-c2ccccc2)c(C(=O)c2ccc(C#N)c2C#N)c1C</chem>
15	<chem>CC(=O)c1cc(C(F)(F)F)c([N+](=O)[O-])c(C#N)c1C#N</chem>
16	<chem>Cc1cc(-c2ccccc2)ccc1OP(=O)(O)Oc1ccc(C#N)c(C#N)c1</chem>
17	<chem>CCc1c(Cl)cc(C#N)c(C#N)c1C(=O)OC</chem>
18	<chem>COC(=O)c1cc(OC)cc(OP(=O)(O)Oc2cccc(C#N)c2C#N)c1O</chem>
19	<chem>COC(=O)c1ccc([N+](=O)[O-])c(C)c1Oc1ccc(Oc2cccc(C#N)c2C#N)cc1</chem>
20	<chem>COC(=O)c1cc(C(=O)OC)c(C(=O)OC)cc1OC(=O)Oc1cccc(C#N)c1C#N</chem>
21	<chem>COC(=O)c1ccc(C(=O)OC)c(Oc2ccc(C#N)c(C#N)c2)c1N</chem>
22	<chem>COC(=O)c1cccc(C)c1O[Si](C)(C)Oc1ccc(C#N)c(C#N)c1</chem>
23	<chem>COC(=O)c1ccc(C(=O)O)c(O[Si](C)(C)Oc2cccc(C#N)c2C#N)c1C(=O)O</chem>
24	<chem>N#Cc1cc(-c2ccccc2)c(C(=O)O)c(S(=O)(=O)O)c1C#N</chem>
25	<chem>N#Cc1ccc(Oc2cc(C(=O)O)cc(-c3ccccc3)c2F)cc1C#N</chem>
26	<chem>Cc1cccc(O[Si](C)(C)Oc2cccc(C#N)c2C#N)c1N</chem>

27	<chem>COC(=O)c1ccc(Sc2ccc(C#N)c(C#N)c2)c(C(=O)O)c1C</chem>
28	<chem>COC(=O)c1ccc(C)c(O[Si](C)(C)Oc2ccc(C#N)c(C#N)c2)c1C(=O)O</chem>
29	<chem>N#Cc1ccc(Oc2ccc(Oc3cc([N+](=O)[O-])c(Cl)cc3-c3ccccc3)cc2)cc1C#N</chem>
30	<chem>CC=CCc1c(C#N)c(C#N)cc(N)c1C(F)(F)F</chem>
31	<chem>COc1cc(OC)c(O[Si](C)(C)Oc2cccc(C#N)c2C#N)c(OC)c1</chem>
32	<chem>COC(=O)c1ccc(O)c(C(=O)OC)c1Oc1cccc(C#N)c1C#N</chem>
33	<chem>N#Cc1ccc(C(=O)c2cccc2-c2cccc2)cc1C#N</chem>
34	<chem>COc1ccc(C(=O)c2cccc(C#N)c2C#N)c(OC)c1F</chem>
35	<chem>COC(=O)c1cc(F)cc(OC(=O)Oc2ccc(C#N)c(C#N)c2)c1C(=O)O</chem>
36	<chem>COc1cc(C(=O)O)c(C(=O)O)cc1OC(=O)Oc1ccc(C#N)c(C#N)c1</chem>
37	<chem>Cc1c(O)ccc(OC(=O)Oc2ccc(C#N)c(C#N)c2)c1Cl</chem>
38	<chem>COC(=O)c1cc(C(=O)OC)cc(C(=O)c2cccc(C#N)c2C#N)c1</chem>
39	<chem>C=Cc1c(O)cc(-c2cccc2)cc1OP(=O)(O)Oc1cccc(C#N)c1C#N</chem>
40	<chem>C=Cc1cc(OC(=O)Oc2cccc(C#N)c2C#N)c([N+](=O)[O-])cc1OC</chem>
41	<chem>C=Cc1cc(-c2cccc2)cc(Cl)c1OP(=O)(O)Oc1ccc(C#N)c(C#N)c1</chem>
42	<chem>COC(=O)c1ccc(F)c(C(=O)c2cccc(C#N)c2C#N)c1Cl</chem>
43	<chem>C=Cc1cccc(C(=O)c2ccc(C#N)c(C#N)c2)c1[N+](=O)[O-]</chem>
44	<chem>C[Si](C)(Oc1cccc(C#N)c1C#N)Oc1cc(-c2cccc2)cc(-c2cccc2)c1[N+](=O)[O-]</chem>
45	<chem>C=Cc1ccc(F)c(OC)c1C(=O)c1ccc(C#N)c(C#N)c1</chem>
46	<chem>COc1ccc(-c2cccc2)c(OP(=O)(O)Oc2cccc(C#N)c2C#N)c1C(=O)O</chem>
47	<chem>COc1cc(Cc2cccc2)c(C#N)c(C#N)c1C(=O)O</chem>
48	<chem>COC(=O)c1cc(O)c(C(=O)c2ccc(C#N)c(C#N)c2)c([N+](=O)[O-])c1</chem>
49	<chem>N#Cc1ccc(OC(=O)Oc2cc(N)c(C(=O)O)c([N+](=O)[O-])c2)cc1C#N</chem>
50	<chem>C=Cc1c(C(=O)OC)ccc(Oc2ccc(Oc3ccc(C#N)c(C#N)c3)cc2)c1N</chem>
51	<chem>N#Cc1cccc(C(=O)c2cccc(F)c2C(=O)O)c1C#N</chem>
52	<chem>COC(=O)c1cc(Oc2cccc(C#N)c2C#N)c(-c2cccc2)cc1C(=O)OC</chem>
53	<chem>Cc1ccc(O)c(C(=O)O)c1OC(=O)Oc1ccc(C#N)c(C#N)c1</chem>
54	<chem>COC(=O)c1c(OP(=O)(O)Oc2ccc(C#N)c(C#N)c2)ccc(Cl)c1C</chem>
55	<chem>COc1ccc(C(=O)O)c(OP(=O)(O)Oc2ccc(C#N)c(C#N)c2)c1O</chem>

56	<chem>COc1cc(C(=O)O)c(O[Si](C)(C)Oc2cccc(C#N)c2C#N)cc1O</chem>
57	<chem>C=CCc1c(C#N)c(C#N)cc(C(F)(F)F)c1Cc1cccc1</chem>
58	<chem>COC(=O)c1cc(C(=O)c2cccc(C#N)c2C#N)c(OC)cc1F</chem>
59	<chem>C=Cc1cc(Oc2cccc(C#N)c2C#N)c([N+](=O)[O-])c([N+](=O)[O-])c1</chem>
60	<chem>Cc1ccc(C(=O)O)c(C)c1OC(=O)Oc1cccc(C#N)c1C#N</chem>
61	<chem>COc1cc(C(C)=O)c(C#N)c(C#N)c1Cc1cccc1</chem>
62	<chem>N#Cc1ccc(OP(=O)(O)Oc2cc(N)c(C(=O)O)c(-c3cccc3)c2)cc1C#N</chem>
63	<chem>C=Cc1cc(C(C)=O)c(Cc2cccc2)c(C#N)c1C#N</chem>
64	<chem>C=Cc1cc(Sc2cccc(C#N)c2C#N)c(-c2cccc2)cc1[N+](=O)[O-]</chem>
65	<chem>N#Cc1cc(Cc2cccc2)c(N)c(Br)c1C#N</chem>
66	<chem>COC(=O)c1cc(C(=O)c2cccc(C#N)c2C#N)c(C)cc1Cl</chem>
67	<chem>C=Cc1cc(Cl)c(O)cc1C(=O)c1ccc(C#N)c(C#N)c1</chem>
68	<chem>Cc1c(Cl)cc(N)cc1Oc1cccc(C#N)c1C#N</chem>
69	<chem>COC(=O)c1ccc(Cl)c(Oc2cccc(C#N)c2C#N)c1F</chem>
70	<chem>COc1ccc(O[Si](C)(C)Oc2ccc(C#N)c(C#N)c2)c(C)c1C(=O)O</chem>
71	<chem>COc1ccc(OC)c(O[Si](C)(C)Oc2cccc(C#N)c2C#N)c1C</chem>
72	<chem>COC(=O)c1cc(F)cc(Oc2ccc(Oc3ccc(C#N)c(C#N)c3)cc2)c1C</chem>
73	<chem>COc1c(-c2cccc2)ccc(Sc2ccc(C#N)c(C#N)c2)c1C</chem>
74	<chem>C=CCc1c(-c2cccc2)cc(C#N)c(C#N)c1O</chem>
75	<chem>C=Cc1cc(N)cc(C(=O)OC)c1Sc1ccc(C#N)c(C#N)c1</chem>
76	<chem>N#Cc1ccc(Cl)c(S(=O)(=O)O)c1C#N</chem>
77	<chem>COc1c(OC(=O)Oc2cccc(C#N)c2C#N)cc(C(=O)O)cc1[N+](=O)[O-]</chem>
78	<chem>COC(=O)c1cccc(Sc2ccc(C#N)c(C#N)c2)c1C(=O)O</chem>
79	<chem>C=Cc1cc(Oc2cccc(C#N)c2C#N)c(OC)cc1O</chem>
80	<chem>C=Cc1cc(F)c(F)cc1C(=O)c1cccc(C#N)c1C#N</chem>
81	<chem>COc1ccc(Oc2ccc(Oc3cccc(C#N)c3C#N)cc2)c(Cl)c1F</chem>
82	<chem>N#Cc1cccc(Sc2cc(O)c(O)cc2O)c1C#N</chem>
83	<chem>C=Cc1cc(C)c(C)c(Sc2cccc(C#N)c2C#N)c1</chem>
84	<chem>C=Cc1cc(O)c(O[Si](C)(C)Oc2cccc(C#N)c2C#N)cc1F</chem>
85	<chem>COc1cc(O)cc([N+](=O)[O-])c1Oc1ccc(C#N)c(C#N)c1</chem>

86	<chem>N#Cc1cccc(Oc2ccc(Oc3cc(N)c(O)cc3[N+](=O)[O-])cc2)c1C#N</chem>
87	<chem>Cc1cc(Cl)cc(Sc2ccc(C#N)c(C#N)c2)c1</chem>
88	<chem>COC(=O)c1ccc(O[Si](C)(C)Oc2ccc(C#N)c(C#N)c2)c([N+](=O)[O-])c1F</chem>
89	<chem>COc1c(-c2ccccc2)ccc(C(=O)O)c1O[Si](C)(C)Oc1cccc(C#N)c1C#N</chem>
90	<chem>COC(=O)c1cc(OC)cc(F)c1Oc1cccc(C#N)c1C#N</chem>
91	<chem>COC(=O)c1c(F)ccc(OC(=O)Oc2ccc(C#N)c(C#N)c2)c1-c1ccccc1</chem>
92	<chem>C=Cc1cc(Oc2cccc(C#N)c2C#N)ccc1-c1ccccc1</chem>
93	<chem>C[Si](C)(Oc1cc(N)c([N+](=O)[O-])c(-c2ccccc2)c1)Oc1cccc(C#N)c1C#N</chem>
94	<chem>COC(=O)c1cc(OP(=O)(O)Oc2cccc(C#N)c2C#N)cc(Cl)c1C</chem>
95	<chem>N#Cc1ccc(Sc2cc(Cl)c(Cl)c([N+](=O)[O-])c2)cc1C#N</chem>
96	<chem>C=Cc1cc(Sc2cccc(C#N)c2C#N)c(F)cc1Cl</chem>
97	<chem>C=Cc1ccc(Cl)c(O[Si](C)(C)Oc2ccc(C#N)c(C#N)c2)c1F</chem>
98	<chem>Cc1c(N)ccc(Cl)c1OP(=O)(O)Oc1ccc(C#N)c(C#N)c1</chem>
99	<chem>COC(=O)c1cc(N)cc(Sc2cccc(C#N)c2C#N)c1C</chem>
100	<chem>C=Cc1ccc(-c2ccccc2)c(O[Si](C)(C)Oc2ccc(C#N)c(C#N)c2)c1F</chem>
101	<chem>COC(=O)c1c(Oc2ccc(C#N)c(C#N)c2)ccc(C)c1C(=O)O</chem>
102	<chem>C[Si](C)(Oc1ccc(C#N)c(C#N)c1)Oc1cc(N)cc([N+](=O)[O-])c1-c1ccccc1</chem>
103	<chem>C=Cc1cc(OC)cc(C(=O)c2ccc(C#N)c(C#N)c2)c1C</chem>
104	<chem>COc1cccc(Cl)c1C(=O)c1ccc(C#N)c(C#N)c1</chem>
105	<chem>COC(=O)c1c([N+](=O)[O-])ccc(Oc2cccc(C#N)c2C#N)c1[N+](=O)[O-]</chem>
106	<chem>COC(=O)c1c(OP(=O)(O)Oc2ccc(C#N)c(C#N)c2)ccc(Cl)c1[N+](=O)[O-]</chem>
107	<chem>COC(=O)c1ccc(OP(=O)(O)Oc2ccc(C#N)c(C#N)c2)c(-c2ccccc2)c1C(=O)O</chem>
108	<chem>COC(=O)c1cc(C#N)c(C#N)c(OC)c1C(=O)OC</chem>
109	<chem>COc1cc([N+](=O)[O-])cc(Sc2ccc(C#N)c(C#N)c2)c1N</chem>
110	<chem>N#Cc1ccc(Oc2ccc(Oc3c(F)ccc(Cl)c3O)cc2)cc1C#N</chem>
111	<chem>N#Cc1cc(C(=O)O)c(F)c(Br)c1C#N</chem>
112	<chem>COc1cc(N)c(Sc2cccc(C#N)c2C#N)c(Cl)c1</chem>
113	<chem>COc1cc(N)cc(Oc2ccc(C#N)c(C#N)c2)c1OC</chem>
114	<chem>Cc1cc(C)c(O)c(Oc2ccc(Oc3ccccc(C#N)c3C#N)cc2)c1</chem>
115	<chem>C[Si](C)(Oc1ccc(C#N)c(C#N)c1)Oc1ccc(Cl)c([N+](=O)[O-])c1</chem>

116	<chem>N#Cc1cccc(C(=O)c2c(C(=O)O)cc(Cl)cc2[N+](=O)[O-])c1C#N</chem>
117	<chem>COc1cccc(C)c1C(=O)c1cccc(C#N)c1C#N</chem>
118	<chem>C=Cc1c(C(=O)OC)ccc(Cl)c1OP(=O)(O)Oc1cccc(C#N)c1C#N</chem>
119	<chem>N#Cc1cc(C(F)(F)F)cc(Cl)c1C#N</chem>
120	<chem>N#Cc1cccc(Oc2c(F)cccc2-c2cccc2)c1C#N</chem>
121	<chem>C=Cc1cc(OC(=O)Oc2ccc(C#N)c(C#N)c2)c(OC)c([N+](=O)[O-])c1</chem>
122	<chem>COC(=O)c1c(Oc2cccc(C#N)c2C#N)cc(OC)cc1[N+](=O)[O-]</chem>
123	<chem>C=Cc1ccc(-c2cccc2)cc1Oc1cccc(C#N)c1C#N</chem>
124	<chem>COC(=O)c1cc(C)cc(C)c1OP(=O)(O)Oc1ccc(C#N)c(C#N)c1</chem>
125	<chem>N#Cc1ccc(Oc2ccc(Oc3c(O)cc(N)cc3O)cc2)cc1C#N</chem>
126	<chem>Cc1ccc(Cl)c(Sc2cccc(C#N)c2C#N)c1Cl</chem>
127	<chem>N#Cc1ccc(Sc2c(N)ccc(F)c2-c2cccc2)cc1C#N</chem>
128	<chem>Cc1cc(C(=O)c2cccc(C#N)c2C#N)c(N)c([N+](=O)[O-])c1</chem>
129	<chem>N#Cc1cc(S(=O)(=O)O)c(-c2cccc2)c([N+](=O)[O-])c1C#N</chem>
130	<chem>CC(C)(C)c1cc(O)c(-c2cccc2)c(C#N)c1C#N</chem>
131	<chem>COC(=O)c1ccc(N)c(Sc2cccc(C#N)c2C#N)c1OC</chem>
132	<chem>CC=CCc1c(C#N)c(C#N)cc(S(=O)(=O)O)c1C(=O)O</chem>
133	<chem>COc1cccc(C(=O)c2ccc(C#N)c(C#N)c2)c1O</chem>
134	<chem>Cc1cc(Oc2ccc(Oc3ccc(C#N)c(C#N)c3)cc2)c(F)cc1F</chem>
135	<chem>C=Cc1cc(-c2cccc2)cc(Oc2ccc(C#N)c(C#N)c2)c1O</chem>
136	<chem>COC(=O)c1ccc(O[Si](C)(C)Oc2cccc(C#N)c2C#N)cc1[N+](=O)[O-]</chem>
137	<chem>COC(=O)c1ccc(C)c(OC(=O)Oc2ccc(C#N)c(C#N)c2)c1-c1cccc1</chem>
138	<chem>COC(=O)c1c(C#N)c(C#N)cc(OC)c1Cc1cccc1</chem>
139	<chem>COC(=O)c1cc([N+](=O)[O-])c(C#N)c(C#N)c1C</chem>
140	<chem>C=CCc1cc(C)c(C=C)c(C#N)c1C#N</chem>
141	<chem>Cc1cc(O[Si](C)(C)Oc2ccc(C#N)c(C#N)c2)cc(-c2cccc2)c1[N+](=O)[O-]</chem>
142	<chem>COC(=O)c1c(C)cc(OC(=O)Oc2ccc(C#N)c(C#N)c2)cc1C</chem>
143	<chem>Cc1c([N+](=O)[O-])ccc([N+](=O)[O-])c1O[Si](C)(C)Oc1cccc(C#N)c1C#N</chem>
144	<chem>CC(C)(C)c1cc(C(=O)Cl)c(F)c(C#N)c1C#N</chem>

145	<chem>COC(=O)c1cc(Oc2ccc(Oc3ccc(C#N)c(C#N)c3)cc2)cc(C(=O)O)c1O</chem>
146	<chem>C=Cc1ccc(C)cc1Oc1ccc(Oc2ccc(C#N)c(C#N)c2)cc1</chem>
147	<chem>N#Cc1ccc(Sc2cc([N+](=O)[O-])c([N+](=O)[O-])c([N+](=O)[O-])c2)cc1C#N</chem>
148	<chem>Cc1cccc(C(=O)c2cccc(C#N)c2C#N)c1C</chem>
149	<chem>N#Cc1c(S(=O)(=O)O)cc(S(=O)(=O)O)c(C(F)(F)F)c1C#N</chem>
150	<chem>C=Cc1c(OC)cc(OC)cc1Oc1ccc(C#N)c(C#N)c1</chem>
151	<chem>C=Cc1c(C#N)c(C#N)cc(C)c1Cc1cccc1</chem>
152	<chem>C=Cc1cc(C(=O)c2ccc(C#N)c(C#N)c2)cc(O)c1C=C</chem>
153	<chem>COc1ccc(-c2cccc2)c(C)c1O[Si](C)(C)Oc1cccc(C#N)c1C#N</chem>
154	<chem>C=Cc1ccc(F)c(Oc2ccc(Oc3ccc(C#N)c3C#N)cc2)c1C(=O)O</chem>
155	<chem>N#Cc1ccc(OC(=O)Oc2c([N+](=O)[O-])cc(C(=O)O)cc2[N+](=O)[O-])cc1C#N</chem>
156	<chem>N#Cc1cccc(OP(=O)(O)Oc2c(O)cc(C(=O)O)cc2-c2cccc2)c1C#N</chem>
157	<chem>C=Cc1cc(OP(=O)(O)Oc2ccc(C#N)c(C#N)c2)cc(C(=O)O)c1C=C</chem>
158	<chem>COC(=O)c1ccc(Oc2cccc(C#N)c2C#N)c(Cl)c1-c1cccc1</chem>
159	<chem>Cc1ccc(Cl)cc1OP(=O)(O)Oc1cccc(C#N)c1C#N</chem>
160	<chem>COC(=O)c1ccc(F)cc1Oc1ccc(C#N)c(C#N)c1</chem>
161	<chem>COc1ccc(OC(=O)Oc2ccc(C#N)c(C#N)c2)cc1C</chem>
162	<chem>N#Cc1ccc(Sc2c(O)ccc(-c3cccc3)c2C(=O)O)cc1C#N</chem>
163	<chem>N#Cc1ccc(Oc2ccc(Oc3cc(N)c(-c4cccc4)c(Cl)c3)cc2)cc1C#N</chem>
164	<chem>COc1cc(OP(=O)(O)Oc2ccc(C#N)c(C#N)c2)c([N+](=O)[O-])cc1-c1cccc1</chem>
165	<chem>C=CCc1cc(C(C)=O)c([N+](=O)[O-])c(C#N)c1C#N</chem>
166	<chem>C=Cc1ccc([N+](=O)[O-])c(OP(=O)(O)Oc2ccc(C#N)c(C#N)c2)c1</chem>
167	<chem>COc1cc(-c2cccc2)c(C(=O)c2cccc(C#N)c2C#N)cc1Cl</chem>
168	<chem>N#Cc1ccc(C(=O)c2cccc2)cc1C#N</chem>
169	<chem>COC(=O)c1cc(C(=O)OC)c(C(=O)c2ccc(C#N)c(C#N)c2)c(C(=O)OC)c1</chem>
170	<chem>C=Cc1cc(OC(=O)Oc2ccc(C#N)c(C#N)c2)c(C(=O)OC)cc1O</chem>
171	<chem>N#Cc1cccc(OP(=O)(O)Oc2ccc(-c3cccc3)cc2O)c1C#N</chem>
172	<chem>COC(=O)c1cc(O)c(OP(=O)(O)Oc2ccc(C#N)c(C#N)c2)c(OC)c1</chem>
173	<chem>CC=CCc1cc(C#N)c(C#N)c(S(=O)(=O)O)c1C(C)(C)C</chem>

174	<chem>COc1cc(F)c(Oc2ccc(Oc3ccc(C#N)c(C#N)c3)cc2)c(-c2ccccc2)c1</chem>
175	<chem>N#Cc1ccc(Oc2ccc(Oc3c(O)cc(-c4ccccc4)cc3Cl)cc2)cc1C#N</chem>
176	<chem>COc1cc(C(=O)O)c(OP(=O)(O)Oc2cccc(C#N)c2C#N)c(C(=O)O)c1</chem>
177	<chem>COC(=O)c1cc(Oc2cccc(C#N)c2C#N)ccc1O</chem>
178	<chem>COC(=O)c1cccc(C(=O)c2ccc(C#N)c(C#N)c2)c1</chem>
179	<chem>N#Cc1ccc(Sc2cc([N+](=O)[O-])cc(C(=O)O)c2C(=O)O)cc1C#N</chem>
180	<chem>N#Cc1ccc(Oc2c(C(=O)O)ccc(N)c2Cl)cc1C#N</chem>
181	<chem>COc1ccc(OC(=O)Oc2ccc(C#N)c(C#N)c2)c(O)c1OC</chem>
182	<chem>COC(=O)c1ccc(C)c(OC(=O)Oc2ccc(C#N)c(C#N)c2)c1</chem>
183	<chem>N#Cc1ccc(Oc2ccc(Oc3cc(C(=O)O)cc(N)c3O)cc2)cc1C#N</chem>
184	<chem>C=Cc1cc(Oc2ccc(Oc3ccc(C#N)c(C#N)c3)cc2)cc(F)c1OC</chem>
185	<chem>COC(=O)c1c(Oc2ccc(Oc3ccc(C#N)c(C#N)c3)cc2)cc(OC)cc1C(=O)O</chem>
186	<chem>COc1cc(OP(=O)(O)Oc2ccc(C#N)c(C#N)c2)c(C)c([N+](=O)[O-])c1</chem>
187	<chem>C=Cc1cc(N)c([N+](=O)[O-])cc1OP(=O)(O)Oc1ccc(C#N)c(C#N)c1</chem>
188	<chem>N#Cc1ccc(OP(=O)(O)Oc2cc(F)cc([N+](=O)[O-])c2Cl)cc1C#N</chem>
189	<chem>N#Cc1cccc(Sc2cc(O)ccc2O)c1C#N</chem>
190	<chem>N#Cc1cccc(Sc2cc(-c3ccccc3)cc(F)c2Cl)c1C#N</chem>
191	<chem>N#Cc1cccc(Oc2cc(N)c(N)cc2-c2ccccc2)c1C#N</chem>
192	<chem>N#Cc1cccc(Oc2ccc(O)c([N+](=O)[O-])c2[N+](=O)[O-])c1C#N</chem>
193	<chem>COC(=O)c1cc(C(=O)c2cccc(C#N)c2C#N)ccc1OC</chem>
194	<chem>COc1c(F)cccc1OC(=O)Oc1cccc(C#N)c1C#N</chem>
195	<chem>Cc1c(F)ccc(O[Si](C)(C)Oc2cccc(C#N)c2C#N)c1-e1ccccc1</chem>
196	<chem>Cc1cc(C(=O)O)cc(OP(=O)(O)Oc2cccc(C#N)c2C#N)c1O</chem>
197	<chem>N#Cc1cccc(OP(=O)(O)Oc2c(C(=O)O)ccc(F)c2-c2ccccc2)c1C#N</chem>
198	<chem>C=Cc1ccc(N)c(OP(=O)(O)Oc2cccc(C#N)c2C#N)c1F</chem>
199	<chem>N#Cc1cc(S(=O)(=O)O)c(S(=O)(=O)O)c(C(F)(F)F)c1C#N</chem>
200	<chem>CC(=O)c1cc(C#N)c(C#N)c(C(=O)O)c1</chem>

4. Molecular Dynamic Simulation of Phthalonitrile Melting Points

All-atomic molecular dynamics (AAMD) simulation has become a reliable tool for predicting material properties due to its advantages of fewer constraints and high flexibility, especially when obtaining original data is challenging. In this study, we conducted all-atomic molecular dynamics simulations to obtain the melting points of 258 phthalonitriles given in sections S1 and S3.

Materials Studio was utilized to build molecular structures and assign/store structural information. Forcite and Dmol3 modules were employed, with Gasteiger rules selected for charge assignment (Qeq was selected alternatively for a small number of situations where Gasteiger was not applicable). Geometry optimization was performed under the Condensed-phase Optimized Molecular Potentials for Atomistic Simulation Studies II (COMPASSII) force field with high computational accuracy (Fine). The Dmol3 module was used for atomic indexing calibration and precalculation, while the exchange-correlation function was set as the commonly used PWC under the LDA.

For each phthalonitrile molecule with a different number of atoms, the structural information was exported from Materials Studio, and Moltemplate was utilized to construct simulation boxes under the Dreiding force field. Moltemplate is frequently employed to generate input files required for AAMD simulations, particularly for the Large-scale Atomic/Molecular Massively Parallel Simulator (LAMMPS) molecular dynamics code. Moltemplate converts information about the molecular system and associated force field parameters into LAMMPS input scripts for direct use in AAMD, simplifying the simulation setup process. It is essential to note that, due to the strict sensitivity of the Dreiding force field to the hybridization of atoms within molecules, careful inspection of the molecular information files generated by Moltemplate is crucial. In this study, all

simulation boxes are imposed by periodic boundary conditions. The total number of atoms in each box was maintained between 8000 and 12000, striking a balance between simulation accuracy and computational efficiency.

LAMMPS was employed for AAMD simulation throughout this study. Unless otherwise specified, the time step in this work is 1 fs. The obtained monomer simulation boxes underwent the following treatment plan. First, a structural optimization (Geometry Optimization) was performed on the simulation box to eliminate internal stresses preliminarily. Subsequently, under the NPT ensemble, a 1 ns relaxation process was applied to achieve further equilibrium and better match the actual density. The recommended pressure (P) and temperature (T) are 500 standard atmospheres and 800K, which can be changed depending on the situation. The pressure must be selected to be relatively high to ensure the volume compression of the simulation box since a substantial box volume would severely degrade simulation efficiency. The temperature was selected to be much higher than the typical melting point of phthalonitriles (approximately 400-550 K), allowing molecules in the box to acquire sufficient kinetic energy for diffusion.

Subsequently, a depressurization process was applied to the relaxed simulation boxes. This is to gradually release pressure throughout the system from high pressure to the final experimental pressure, which is one atmosphere. The depressurization operation must be uniform, and the entire process must be distributed over an extended interval to avoid system damage or imbalance caused by abrupt pressure drops. In this work, the depressurization process was completed within 1 ns. Similarly, uniformly decreasing the temperature from high to the testing temperature is necessary. Here, the cooling process was completed within 600 ps.

Generally, their density suddenly decreases when most substances undergo a transition from solid to liquid. This is because the molecular arrangement in the solid state is more tightly packed compared to the liquid state. In other words, during the melting phase transition, there is a sudden change in the substance density, manifested as a turning point in the temperature-density plot. Therefore, by observing the turning point in the temperature-density plot of a substance, its melting point can be determined. This method has been proven applicable in several studies^[27, 28].

Based on this, we designed a wide temperature range for each studied phthalonitrile molecule, ensuring that the melting point of the phthalonitrile will fall within this range. We refer to this range as the experimental temperature range, which is recommended to be from 240 K to 700 K and can be changed depending on the situation. We divided the entire experimental temperature range into intervals of 20 K, obtaining several experimental temperatures. Starting from high to low temperature, we performed a 700 ps dynamic equilibrium in the NPT ensemble at each testing temperature under one standard atmosphere. The system is expected to reach equilibrium within the first hundreds of ps, and then in the last 200 ps, we took the average of the last 100 recorded system densities as the density we need at the current temperature. Collecting densities at all experimental temperatures yields a density-temperature plot. Fitting the plot piecewisely reveals the turning points, indicating the melting point of the current phthalonitrile. It is worth noting that a cooling process is more favorable than a heating process. It ensures that the substance undergoes phase transition while changing from high to low temperature, ensuring that molecules have as much kinetic energy as possible for motion and rearrangement. Additionally, the temperature range setting can be flexibly adjusted to observe an apparent turning point in the plot.

5. Gaussian Process Regression

Gaussian Process Regression (GPR) can be employed as a surrogate model for the black-box function representing material properties. We can view the Gaussian process as a distribution over the function space.

Consider an input space \mathbf{X} and an output space \mathbf{Y} . For any set of points $\mathbf{X}=\{x_1, x_2, \dots, x_n\}$ in the input space, the corresponding points $\mathbf{Y}=\{y_1, y_2, \dots, y_n\}$ in the output space follow a multi-dimensional Gaussian distribution. Thus, the distribution of the entire function space can be described as a Gaussian process. In GPR, we consider the output y corresponding to an input x as a random variable following a Gaussian distribution. For a given input point x , we have:

$$y = f(x) + \varepsilon \quad (\text{S1})$$

Here, $f(x)$ is the unknown function representing the relationship we aim to model, and ε is a zero-mean noise term used to account for the randomness in the observed data.

Before observing any data, we have a prior distribution over the function space. Typically, this prior distribution is assumed to have a mean of zero, and the covariance is determined by the chosen kernel function. The kernel function defines the similarity between input points, *i.e.*, the covariance matrix.

$$f(x) \sim GP[0, k(x, x')] \quad (\text{S2})$$

Once observational data is available, we can update our estimation of the function space through Bayesian inference. The observed data, denoted as $\mathbf{D}=\{(x_1, y_1), (x_2, y_2), \dots, (x_n, y_n)\}$, is assumed to be generated from the true function $f(x)$ with added noise. The relationship between the observed data and the prior distribution can be expressed by

$$y_i = f(x_i) + \varepsilon_i \quad (\text{S5-3})$$

By utilizing observational data, we can compute the posterior distribution, representing an updated estimation of the function space based on the observed data. The mean and variance of the posterior distribution change as more observational data becomes available. For a new input x^* , we can predict the corresponding output y^* using the posterior distribution. The predictive distribution includes the expected value of the output and also provides an estimate of the predictive uncertainty.

This process allows us to model the function space flexibly and obtain uncertainty estimates in predictions, particularly useful in practical applications. The GRP is commonly used in ML to model complex relationships between inputs and outputs. As a non-parametric method, it does not require assumptions about the form of the function, making it suitable for complex nonlinear relationships, and it performs well in regression problems with high noise and small sample sizes. In practice, choosing appropriate kernel functions and adjusting corresponding hyperparameters is crucial.

6. Constructing Models by Gaussian Process Regression

Data with different precisions were utilized for ML here to obtain low- and high-fidelity models. The high-fidelity model may be more accurate but comes with higher costs, while the low-fidelity model costs less but is relatively inaccurate. When identifying a specific relationship, we employed the low-fidelity model for initial exploration and delved deeper with a high-fidelity model to expedite the process. This approach can perform more efficiently when resources are limited and holds potential significance in fields such as high-throughput research and efficient material discovery.

We obtained a comprehensive set of 517-dimensional valid descriptors for 258 phthalonitrile structures using the Mordred tool. We performed a dimensionality reduction on descriptors to avoid excessively low ML efficiency. We directly calculated the correlation coefficients between each descriptor and the target value (melting point), selecting descriptors with the highest correlation as the dimensionality reduction result. All descriptors were reduced to 23 dimensions, along with simulated melting points, to form the low-fidelity dataset for learning $Y_L(\mathbf{X})$. The selected kernel functions included Matern(0.5), Matern(1.5), Matern(2.5), and RBF. Throughout the process, models constructed using each kernel function were iterated 500 times, resulting in a total of 2000 models. In each learning iteration, the dataset was split into training, validation, and test sets in a ratio of 7:2:1. The training set was utilized to obtain a reasonable posterior distribution, and the validation set was used to monitor the learning process and prevent overfitting. Here, we utilized the performance on the validation set to judge the performance of the low-fidelity model. R^2 , MAE, and MSE of all models were calculated, which is shown in Table S5. Naturally, the model with high R^2 and

relatively low MAE and MSE can be regarded as the optimal model, *i.e.*, the $Y_L(\mathbf{X})$ we seek.

Then, we utilized the structures of 58 phthalonitriles collected from literature and the mathematical differences between their simulated and experimental melting points as a dataset for ML. The Leave-one-out cross-validation (LOO) was employed to obtain the optimal $Y_D(\mathbf{X})$ model. Subsequently, the previous $Y_L(\mathbf{X})$ was combined with $Y_D(\mathbf{X})$ to form the $Y_H(\mathbf{X})$ model. At the same time, we employed the same method to construct the experimental value model $Y_E(\mathbf{X})$ as a control group using the pure experimental melting point as the dataset. The performance of the optimal model of $Y_L(\mathbf{X})$, $Y_H(\mathbf{X})$, and $Y_E(\mathbf{X})$ are listed in Tables S6 and S7.

Supplementary Table 5 R^2 of the best $Y_L(\mathbf{X})$ model on the training and validation sets using various kernels

Kernels	Training	Validation
Matern(0.5)	0.783	0.605
Matern(1.5)	0.659	0.602
Matern(2.5)	0.641	0.595
RBF	0.632	0.582

Supplementary Table 6 Performance of the optimal $Y_L(\mathbf{X})$ model

Kernels	MAE	MSE	R^2
Matern(0.5)	20.747	683.271	0.605

Supplementary Table 7 Performance of the optimal $Y_H(\mathbf{X})$ and $Y_E(\mathbf{X})$ model

Kernels	R^2		MAE (K)	
	$Y_H(\mathbf{X})$	$Y_E(\mathbf{X})$	$Y_H(\mathbf{X})$	$Y_E(\mathbf{X})$
Matern(0.5)	0.836	0.562	20.125	41.264
Matern(1.5)	0.836	0.488	20.067	44.139
Matern(2.5)	0.836	0.478	20.041	44.442
RBF	0.836	0.467	20.032	44.726

We also applied other dimensionality reduction methods, such as PCA and RFE, for comparison. It was found that the dimensionality reduction effect of RFE was not as practical as our selected method, while the effect of PCA was significantly worse. This is likely because PCA, an unsupervised learning method, does not utilize melting point information during dimensionality reduction, making it less sensitive to this property. The reasonable choice of dimensionality reduction methods is critical to ensuring that descriptors that fully represent material properties are identified, which has a crucial impact on the accuracy of predictive models.

7. Graph Machine Learning, MPNN and MEGNet

Graph machine learning is an ML category specializing in processing and analyzing graph-structured data. In GML, data is represented as a graph, where nodes and edges represent entities and relationships, respectively. This graph structure is applicable for modeling various intricate relationships and networks, and as a result, it has found widespread applications in many fields. The main methods in GML include Graph Neural Networks (GNNs), Graph Convolutional Networks (GCNs), Graph Attention Networks (GATs), and others. GML does not have strict requirements on data scale and is particularly suitable for handling data with intricate relationships and structures due to the ability to model complex relationships between entities. Moreover, since graph structures have the capability of message passing and a certain degree of versatility, GML performs well in performance prediction, and models generated have been proven to possess strong generalization capabilities. In materials science, GML has been employed widely for material discovery and performance prediction^[29, 30], and still holds potential to be exploited.

The MPNN framework originates from the work of Gilmer et al.^[31] in 2017. In general, the basic workflow of the complete MPNN framework includes steps such as Graph Representation, Message Passing, Update, Pooling, and Readout. The MEGNet algorithm employed in this work is a generalization or superset of MPNN^[32]. We can summarize the whole process into the following three steps.

Graph Representation. Graph representation is a crucial initial step in all GML applications. Typically, undirected graphs are used to represent molecular structures. An undirected graph (**G**) is a data structure consisting of vertices (**V**) and edges (**E**). In chemistry, atoms are represented as

vertices and chemical bonds are represented by edges connecting two vertices. The term "atom" may encompass attributes such as atomic number, space coordinates, valence, charge, and so on. Similarly, the "chemical bond" may encompass attributes like bond type, bond connectivity, and bond energy. Therefore, we can use a vertex feature matrix (atom information matrix) to store the attribute information for each atom and an edge feature matrix (bond information matrix) to store the attribute information for chemical bonds. An adjacency matrix records whether a chemical bond connects two atoms.

In this work, MEGNet accepts a molecular graph $\mathbf{G} = (\mathbf{V}, \mathbf{E}, \mathbf{u})$ as input, where \mathbf{V} is the atom information matrix, \mathbf{E} is the bond information matrix, and \mathbf{u} represents the global state attribute. After importing the "Phthalonitrile SMILES-Melting Point" dataset for input, \mathbf{V} and \mathbf{E} are calculated using the OpenBabel and NetworkX packages. Attributes of atom, bond, and global state involved in this work are listed in Table S8. The final molecular graph can be represented as a set: {Atom information matrix (Atom), Bond information matrix (Bond), Global state array (State), Bond index array 1 (Index 1), Bond index array 2 (Index 2)} (Index 1 and Index 2 are obtained from the bond information through attribute matrix concatenation, undirected graph conversion, and ascending index operations for subsequent bond information processing).

Supplementary Table 8 Atom, chemical bond, and global state attributes in this work

Matrix	Attribute
Atom information matrix (Atom)	Element
	Chirality
	Formal_charge
	Ring_sizes
	Hybridization
	Donor
	Acceptor
	Aromatic
Bond information matrix (Bond)	Bond_type
	Same_ring
	Graph_distance
	Spatial_distance
Global state attribute (State)	0
	1

Message Passing and Update. Upon receiving the graph input $\mathbf{G} = (\mathbf{V}, \mathbf{E}, \mathbf{u})$, the model extracts features from graph vertices, edges, and global state attributes through multiple stacked MEGNet blocks, facilitating the message-passing process. This is achieved by utilizing update functions. First, bond attributes are updated with information flowing in from the bond information matrix, atom information matrix, and global state attribute, resulting in new bond attributes. Then, atom attributes and global variable attributes are updated similarly. The ultimate output is a new graph representation $\mathbf{G} = (\mathbf{V}', \mathbf{E}', \mathbf{u}')$.

Message Readout. MEGNet employs a message readout module based on the seq2seq neural network^[f] recommended by the MPNN framework. This module is responsible for the readout of

information from the updated atom information matrix and bond information matrix after message passing and is proven to possess better inductive capabilities of graph features. Seq2seq can be broadly divided into basic units such as the Reading, Process, and Writing blocks. Execution details of each block can be referred to references [33] for more information.

All parameter settings and model evaluation performance in MAGNet are listed in Tables S8-S12.

Supplementary Table 9 Hyperparameter value settings in five-fold cross-validation

Learning rate	Epoch	Batch size
0.0001, 0.0005, 0.0008, 0.001	1000, 2000, 3000	2, 4, 8, 16, 32

Supplementary Table 10 Optimal hyperparameter combination obtained by five-fold cross-validation

Learning rate	Epoch	Batch size
0.0008	2000	4

Supplementary Table 11 Validation performance with the optimal hyperparameter in five-fold

cross-validation

Learning rate_Batch size_Epoch_Number	RMSE (K)	MAE (K)	R²
0.0008_4_2000_1	21.335	16.771	0.923
0.0008_4_2000_2	15.899	12.452	0.926
0.0008_4_2000_3	25.003	13.994	0.829
0.0008_4_2000_4	19.040	10.267	0.926
0.0008_4_2000_5	20.514	11.825	0.914
Average	20.358	13.062	0.904

Supplementary Table 12 Performance of the MEGNet model under the optimal hyperparameter

combination

RMSE		MAE		R²	
Training set	Test set	Training set	Test set	Training set	Test set
12.867	20.911	8.271	14.183	0.934	0.925

References

- [1] Laskoski M, Neal A, Keller T M, et al. Improved synthesis of oligomeric phthalonitriles and studies designed for low temperature cure[J]. *Journal of Polymer Science Part A: Polymer Chemistry*, 2014, 52(12): 1662-1668.
- [2] Dominguez D D, Keller T M. Low-melting phthalonitrile oligomers: preparation, polymerization and polymer properties[J]. *High Performance Polymers*, 2006, 18(3): 283-304.
- [3] Bulgakov B A, Sulimov A V, Babkin A V, et al. Phthalonitrile-carbon fiber composites produced by vacuum infusion process[J]. *Journal of Composite Materials*, 2017, 51(30): 4157-4164.
- [4] Weng Z, Hu Y, Qi Y, et al. Enhanced properties of phthalonitrile resins under lower curing temperature via complex curing agent[J]. *Polymers for Advanced Technologies*, 2020, 31(2): 233-239.
- [5] Yakovlev M V, Morozov O S, Afanaseva E S, et al. Trifunctional thermosetting monomer with propargyl and phthalonitrile groups[J]. *Russian Chemical Bulletin*, 2020, 69: 2183-2190.
- [6] Zhang Z, Li Z, Zhou H, et al. Self - catalyzed silicon - containing phthalonitrile resins with low melting point, excellent solubility and thermal stability[J]. *Journal of Applied Polymer Science*, 2014, 131(20).
- [7] Han Y, Tang D, Wang G, et al. Low melting phthalonitrile resins containing methoxyl and/or allyl moieties: synthesis, curing behavior, thermal and mechanical properties[J]. *European Polymer Journal*, 2019, 111: 104-113.
- [8] Hu J, Xie H, Zhu Z, et al. Reducing the melting point and curing temperature of aromatic

- cyano-based resins simultaneously through a Brønsted acid-base synergistic strategy[J]. *Polymer*, 2022, 246: 124745.
- [9] Monzel W J, Lu G Q, Pruyt T L, et al. Thermal and oxidative behavior of a tetraphenylsilane-containing phthalonitrile polymer[J]. *High Performance Polymers*, 2019, 31(8): 935-947.
- [10] Wu M, Xu J, Bai S, et al. A high-performance functional phthalonitrile resin with a low melting point and a low dielectric constant[J]. *Soft matter*, 2020, 16(7): 1888-1896.
- [11] Yang G, Lv J, Zeng K, et al. The preparation of phthalonitrile monomer and resin containing parylene structure: CN202110602375.5[P].CN202110602375.5[2024-01-09].
- [12] Liu C, Zhang B, Sun M, et al. Novel low-melting bisphthalonitrile monomers: synthesis and their excellent adhesive performance[J]. *European Polymer Journal*, 2021, 153: 110511.
- [13] Bai S, Sun X, Chen X, et al. Synthesis and properties of a thioether bonded phthalonitrile resin[J]. *Materials Today Communications*, 2020, 24: 101352.
- [14] Hu J, Yang W, Tan W, et al. A novel development route for cyano-based high performance thermosetting resins via the strategy of functional group design-dicyanoimidazole resins[J]. *Polymer*, 2020, 203: 122823.
- [15] Nechausov S S, Aleksanova A A, Morozov O S, et al. Low-melting phthalonitrile monomers containing maleimide group: Synthesis, dual-curing behavior, thermal and mechanical properties[J]. *Reactive and Functional Polymers*, 2021, 164: 104932.
- [16] Jia Y, Bu X, Dong J, et al. Catalytic polymerization of phthalonitrile resins by carborane with enhanced thermal oxidation resistance: Experimental and molecular simulation[J]. *Polymers*, 2022, 14(1): 219.

- [17] Zhang H, Yan Z, Yang Z, et al. Synthesis, curing and thermal properties of the low melting point phthalonitrile resins containing glycidyl groups[J]. *Polymer Bulletin*, 2023, 80(1): 725-738.
- [18] Keller T M, Sastri S B. Phthalonitrile prepolymerization composition: U.S. Patent 6,297,298[P]. 2001-10-2.
- [19] Zhou H, Liu F, Li X, et al. Preparation of ortho-, meta-, and para- self-catalyzed cyanate resins and comparative study of their relevant properties[C]. *The 16th National Academic Annual Conference on Composite Materials*, 2010.
- [20] Liu F, Li X. Preparation and thermal properties of novel self-catalyst resin with cyano group[J]. *Aerospace Materials & Technology*, 2010, 40(2): 45-48.
- [21] Wang H, Wang J, Guo H, et al. A novel high temperature vinylpyridine-based phthalonitrile polymer with a low melting point and good mechanical properties[J]. *Polymer Chemistry*, 2018, 9(8): 976-983.
- [22] Wu M, Yang K, Li Y, et al. A pyridazine-containing phthalonitrile resin for heat-resistant and flame-retardant polymer materials[J]. *Polymers*, 2022, 14(19): 4144.
- [23] Tararykina T V, Maizlish V E, Galanin N E, et al. 4-acyloxy-and 4-acylaminophthalonitriles and phthalocyanines based thereon[J]. *Russian Journal of Organic Chemistry*, 2007, 43: 1719-1725.
- [24] Milaeva E R, Kolnin S D, Petrosyan V S. Synthesis of tetrasubstituted acylaminophthalocyanines of cobalt[J]. *Russian chemical bulletin*, 1996, 45: 2027-2028.
- [25] Hu J, Xie H, Zhu Z, et al. Reducing the melting point and curing temperature of aromatic

- cyano-based resins simultaneously through a Brønsted acid-base synergistic strategy[J]. *Polymer*, 2022, 246: 124745.
- [26] Wang W, Jiang X, Tian S, et al. Automated pipeline for superalloy data by text mining [J]. *npj Computational Materials*, 2022, 8(1): 9.
- [27] Liu N, Zeman S, Shu Y, et al. Comparative study of melting points of 3, 4-bis (3-nitrofurazan-4-yl) furoxan (DNTF)/1, 3, 3-trinitroazetidine (TNAZ) eutectic compositions using molecular dynamic simulations[J]. *RSC advances*, 2016, 6(64): 59141-59149.
- [28] Ren F, Shi W, Cao D, et al. A theoretical investigation into the cooperativity effect on the TNT melting point under external electric field[J]. *Journal of Molecular Modeling*, 2021, 27: 1-11.
- [29] Antoniuk E R, Li P, Kailkhura B, et al. Representing Polymers as Periodic Graphs with Learned Descriptors for Accurate Polymer Property Predictions[J]. *Journal of Chemical Information and Modeling*, 2022, 62(22): 5435-5445.
- [30] Sumpter B G, Noid D W. Neural networks and graph theory as computational tools for predicting polymer properties [J]. *Macromolecular Theory and Simulations*, 1994, 3(2): 363-378.
- [31] Gilmer J, Schoenholz S S, Riley P F, et al. Neural message passing for quantum chemistry[C]. *International conference on machine learning*. PMLR, 2017: 1263-1272.
- [32] Vinyals O, Bengio S, Kudlur M. Order matters: Sequence to sequence for sets[J]. *arXiv preprint arXiv:1511.06391*, 2015.
- [33] Chen C, Ye W, Zuo Y, et al. Graph networks as a universal machine learning framework for molecules and crystals[J]. *Chemistry of Materials*, 2019, 31(9): 3564-3572.